

## Supplementary Information

### **Mimicking the brain functions of learning, forgetting and explicit/implicit memories with SrTiO<sub>3</sub>-based memristive devices**

*Xue-Bing Yin<sup>1</sup>, Rui Yang<sup>1\*</sup>, Kan-Hao Xue<sup>2</sup>, Zheng-Hua Tan<sup>1</sup>, Xiao-Dong Zhang<sup>1</sup>, Xiang-Shui Miao<sup>2</sup>, and Xin Guo<sup>1\*</sup>*

1. Laboratory of Solid State Ionics, School of Materials Science and Engineering, Huazhong University of Science and Technology, Wuhan 430074, P.R. China

2. Wuhan National Laboratory for Optoelectronics, School of Optical and Electronic Information, Huazhong University of Science and Technology, Wuhan 430074, P.R. China

## S1 Effect of amplitude

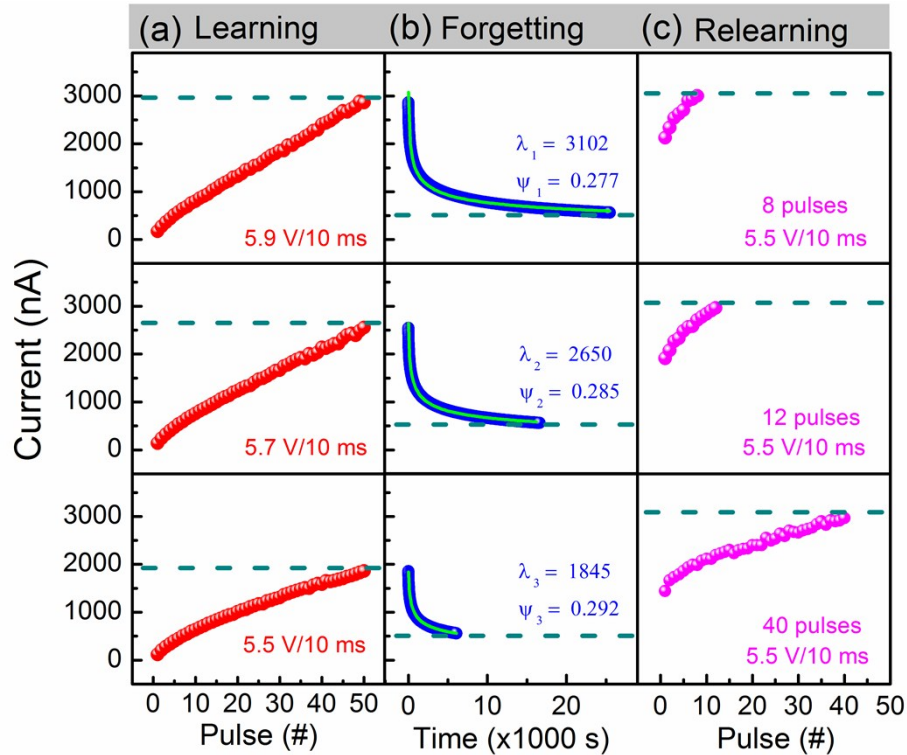


Fig. S1 Effect of the implicit memory on the relearning process by changing the amplitude of the pulses in the first learning process. (a) The device conductance increased to different values by applying same numbers of electric pulses with different amplitudes in the first learning period. (b) The spontaneous current decays was set to decrease to the same level. (c) Different numbers of pulses were used to stimulate the device to the same current level in the relearning period.

The learning strength can be modulated by adjusting the amplitude of the stimulus pulses applied in the first learning period, as presented in Fig. S1. First of all, different levels of learning strength (with device currents of  $\sim 2000$  nA,  $\sim 2600$  nA and  $\sim 3000$  nA, respectively) were obtained in the first learning period by applying same numbers (50) of stimulus pulses with different amplitudes (5.5 V/10 ms, 5.7 V/10 ms and 5.9 V/10 ms, respectively), as shown in Fig. S1(a). The device currents were then allowed to decay to the same level of  $\sim 500$  nA,

corresponding to different lapses of the explicit memory, as shown in Fig. S1(b). Then pulses with the same amplitude (5.5 V/10 ms) were imposed onto the device to increase the current to the same level of  $\sim 3000$  nA, as shown by the relearning curves in Fig. S1(c). It can be seen that stimulating the device with higher amplitude in the first learning period leads to a higher level of the learning strength, which results in a longer period of the explicit memory loss and requires less rehearsal to reach the same learning level in the relearning period. Such a decrease of the pulse number in the relearning period indicates the “time-saving” effect of the implicit memory as well.

## S2 *Ab initio* calculation

### S2-1 Bulk

To disclose the electron trapping/detrapping, we carried out *ab initio* calculation. Here we considered oxygen vacancies as the main defect state, because the defect structure of SrTiO<sub>3</sub> is dominated by oxygen vacancies. All calculations were conducted using the density function theory<sup>1,2</sup> as implemented in the plane-wave based Vienna *ab initio* Simulation Package (VASP),<sup>3,4</sup> while the plane wave cutoff energy was 425 eV. The generalized gradient approximation (GGA) was adopted for the exchange-correlation energy, within the PBEsol form<sup>5</sup> which generally yields good lattice parameters. Considered valence electrons were: 4s, 4p and 5s for Sr; 3s, 3p, 3d and 4s for Ti; 2s and 2p for O; 3d and 4s for Ni. Core electrons were approximated by projector augmented-wave pseudopotentials.<sup>6,7</sup> By fitting to the third order Birch–Murnaghan equation of state, the equilibrium lattice constant for SrTiO<sub>3</sub> was calculated to

be 3.8974 Å and the bulk modulus 183.6 GPa. These are very close to the experimental values of 3.89 Å and 179 GPa.<sup>8</sup>

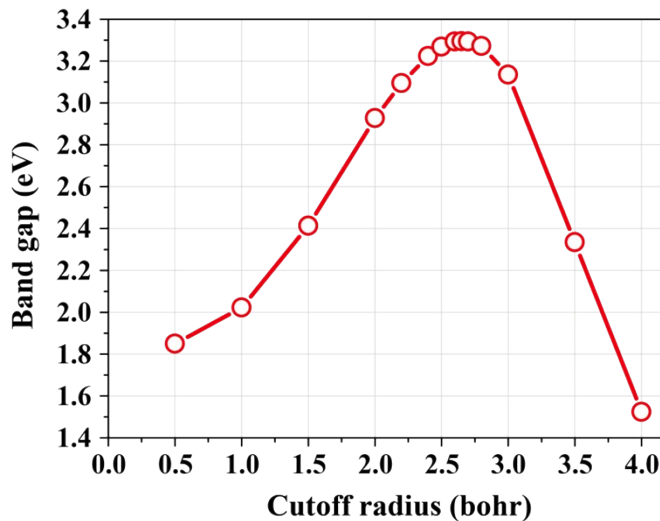


Fig. S2-1 Procedure to determine the optimal cutoff radius for oxygen anion in SrTiO<sub>3</sub>, as carried out for GGA-1/2. The particular cutoff radius leading to the maximal band gap can be selected unambiguously, i.e., 2.65 bohr.

The Schottky barrier height relies on an accurate electronic band structure of the semiconductor. GGA is insufficient in this aspect, because it usually predicts a band gap much smaller than the experimental value. Some computationally expensive methods such as hybrid functionals<sup>9</sup> and the quasi-particle approach with the GW approximation<sup>10</sup> may yield good band gaps, but they cannot be applied to a large supercell with more than 100 atoms. Hence, we adopted the GGA-1/2 approach proposed by Ferreira *et al.*,<sup>11,12</sup> which predicts correct band gaps for many semiconductors but only requires equivalent computational loads as GGA. In the SrTiO<sub>3</sub> case, we stripped 1/2 electron from each O anion and added the self-energy potential back to the O pseudopotential file. The self-energy potential was trimmed by a step-function at

some particular cutoff radius to avoid energy divergence, where the correct cutoff radius should yield a maximal band gap. The as-calculated band gaps with respect to cutoff radii are shown in Fig. S2-1, and at 2.65 bohr the band gap is maximized. Hence, there is no empirical parameter in this variation procedure and 3.29 eV is the unique band gap result corresponding to this optimized cutoff radius. This is a substantial improvement over the conventional GGA, which only gives a 1.82 eV band gap, far below the experimental value of 3.25 eV.

### S2-2 Ni/SrTiO<sub>3</sub> interface

For simplicity, we did the *ab initio* calculation for a simplified model of Ni(100)/SrTiO<sub>3</sub>(100) interface. Such a simple model still gives us some insight into the Schottky barrier. Metallic Ni has a face-centered cubic structure with a lattice constant (3.52 Å) slightly smaller than that of SrTiO<sub>3</sub> (3.89 Å). To retain the band structure, Ni should be expanded to fit the lattice of SrTiO<sub>3</sub>. The interface region is constructed with Ni(100) and SrTiO<sub>3</sub>(100) surfaces for simplicity. Several Ni/SrTiO<sub>3</sub> interface models with different atomistic matches were tested and the energetically most favorable stoichiometric model is illustrated in Fig. S2-2. In the model supercell, atomic coordinates were relaxed until all Hellmann-Feynman forces were below 0.04 eV/Å. A 5×5×1 Monkhorst-Pack k-mesh were used to sample the Brillouin zone during GGA structural relaxation and a 9×9×3 k-mesh was used to calculate the electronic density of states (DOS) using GGA-1/2. The Schottky barrier height is determined by examining the local DOS within each layer. As shown in Fig. S2-2, the conduction band edge deep in SrTiO<sub>3</sub> is 0.46 eV above the Fermi level.

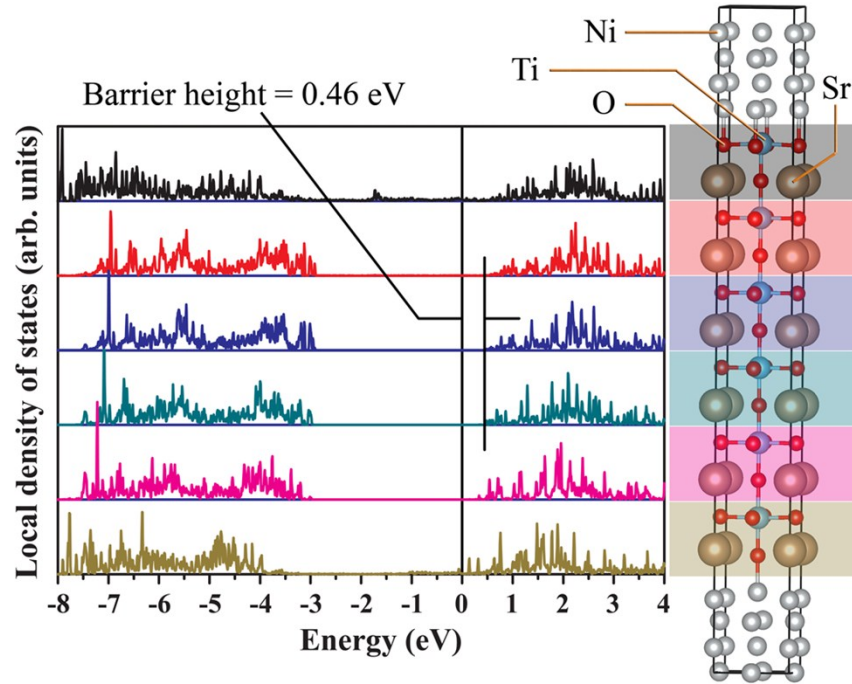


Fig. S2-2 Local density of state (LDOS) analysis for various SrTiO<sub>3</sub> layers in the Ni/SrTiO<sub>3</sub> interface model. Each LDOS curve is aligned vertically to its corresponding layer, while the Fermi level is set to zero in all cases.

For cubic SrTiO<sub>3</sub> with an equilibrium lattice constant [Fig. S2-3(a)], the electronic band structure calculation by GGA-1/2 yields a band gap of 3.29 eV, agreeing with the experimental value of 3.25 eV very well.<sup>13</sup> In contrast, the GGA band gap is much too low as compared in Fig. S2-3(b). The Schottky barrier height can be derived by checking the local density of states in various layers of SrTiO<sub>3</sub>, which gives 0.46 eV. Since Ni is stressed, its work function is subject to modification. We thus calculated the metallic Ni with stressed lattice parameters, and found its work function to be 4.93 eV, being 0.22 eV lower than the experimental value of 5.15 eV. This implies that the Schottky barrier height between Ni and SrTiO<sub>3</sub> might be close to 0.7 eV. Subsequently, we constructed a 184-atom Ni-SrTiO<sub>3</sub> supercell with a volume of 7.79×7.79×33.91 Å for defect investigation. An oxygen vacancy ( $V_O$ ) was introduced at the

bottom interface and the relaxed structure is illustrated in the central part of Fig. S2-3(c). For a neutral vacancy, the barrier height decreases to c.a. 0.1 eV, as determined from the local DOS analysis in the left part of Fig. S2-3(c). However, when the oxygen vacancy is +2 charged, i.e., missing the trapped electrons, the barrier height recovers to c.a. 0.5 eV [right part of Fig. S2-3(c)]. Hence, through electron trapping/detrapping, the Schottky barrier height at the Ni/SrTiO<sub>3</sub> interface can switch between 0.1 eV and 0.5 eV. Since the work function of Ni is underestimated by ~0.22 eV, these barrier heights are quite close to values experimentally derived for ON- and OFF-states (~0.5 eV for the ON-state, ~0.72 eV for the OFF-state).<sup>14</sup>

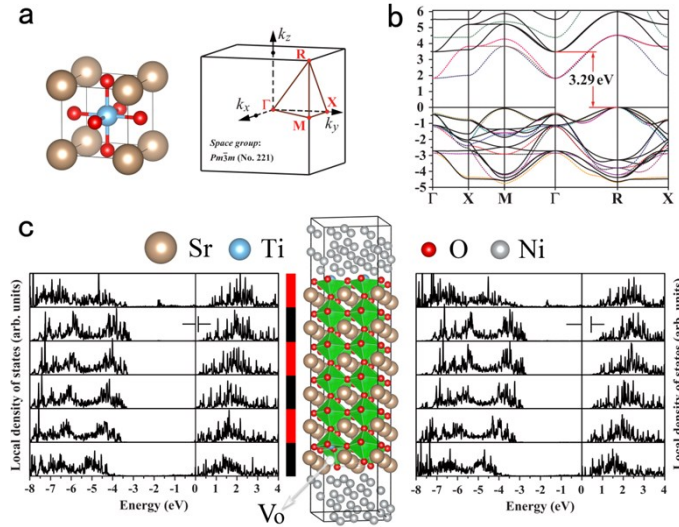


Fig. S2-3 *Ab initio* calculation results. (a) Atomic structure and the first Brillouin zone of cubic SrTiO<sub>3</sub>. (b) Comparison of GGA and GGA-1/2 band structures for cubic SrTiO<sub>3</sub>, where dotted color curves represent GGA results and solid black curves represent GGA-1/2 results. (c) Local density of states (LDOS) for various layers of SrTiO<sub>3</sub> in the Ni/SrTiO<sub>3</sub> interface model. An oxygen vacancy ( $V_O$ ), either neutral (LDOS shown in the left diagram) or +2 charged (LDOS shown in the right diagram), is introduced at the bottom interface. Each curve in the LDOS diagrams is aligned to its corresponding atomic layer along the vertical direction. Since only the

Ni/SrTiO<sub>3</sub> interface is concerned here, two identical interfaces are constructed to avoid the insertion of a vacuum layer, which is a common practice in interface calculations.

## References

1. P. Hohenberg and W. Kohn, *Phys. Rev.*, 1964, **136**, B864–B871.
2. W. Kohn, L. J. Sham, *Phys. Rev.*, 1965, **140**, A1133–A1138.
3. G. Kresse and J. Furthmüller, *Comput. Mater. Sci.*, 1996, **6**, 15–50.
4. G. Kresse and J. Furthmüller, *Phys. Rev. B*, 1996, **54**, 11169–11186.
5. J. P. Perdew, A. Ruzsinszky, G. I. Csonka, O. A. Vydrov, G. E. Scuseria, L. A. Constantin, X. Zhou and K. Burke, *Phys. Rev. Lett.*, 2008, **100**, 136406.
6. P. E. Blöchl, *Phys. Rev. B*, 1994, **50**, 17953–17979.
7. G. Kresse and D. Joubert, *Phys. Rev. B*, 1999, **59**, 1758–1775.
8. K. H. Hellwege, A. M. Hellwege, *Landolt-Börnstein New Ser. Group III Vol 3 Springer Verl. Berl.* 1969, 2001, **90**, 6156–6164.
9. J. Heyd, G. E. Scuseria and M. Ernzerhof, *J. Chem. Phys.*, 2003, **118**, 8207–8215.
10. L. Hedin, *Phys. Rev.*, 1965, **139**, A796–A823.
11. L. G. Ferreira, M. Marques and L. K. Teles, *Phys. Rev. B*, 2008, **78**, 125116.
12. L. G. Ferreira, M. Marques and L. K. Teles, *AIP Adv.*, 2011, **1**, 032119.
13. K. Van Benthem, C. Elsässer and R. French, *J. Appl. Phys.*, 2001, **90**, 6156.
14. X.-B. Yin, Z.-H. Tan and X. Guo, *Phys. Chem. Chem. Phys.*, 2015, **17**, 134-137.